Safety Evaluation of All-Solid-State Batteries: An Innovative Methodology Using In Situ Synchrotron X-ray Radiography

Juliette Charbonnel, Natacha Darmet, Claire Deilhes, Ludovic Broche, Magali Reytier, Pierre-Xavier Thivel, Rémi Vincent

Title:

Safety evaluation of all-solid-state batteries: an innovative methodology using in-situ synchrotron x-ray radiography

By Juliette Charbonnel (1&2), Natacha Darmet (1), Claire Deilhes (1), Ludovic Broche (3), Magali Reytier (1), Pierre-Xavier Thivel (2) and Rémi Vincent* (1).

The email address are respectively : juliette.charbonnel@cea.fr, natacha.darmet2@cea.fr , claire.deilhes@gmail.com, broche.ludovic@gmail.com, magali.reytier@cea.fr, pierre-xavier.thivel@univ-grenoble-alpes.fr and remi.vincent@cea.fr.

1 University Grenoble Alpes, CEA, LITEN, DEHT, F-38000 Grenoble, France
2 University Grenoble Alpes, University Savoie Mont Blanc, CNRS, Grenoble INP, LEPMI, F-38000 Grenoble, France

3. European Synchrotron Radiation Facility (ESRF), 38000 Grenoble, France

Abstract:

All-solid-state battery (ASSB) are expected to be a relevant solution to increase the energy density in lithium-ion battery (LiB) technology. However, the energy management requires high-energy storage capacities, which makes the safety a crucial issue. Unfortunately, it is difficult so far to assess safety of non-fully mature battery technologies. In this paper, we describe a methodology to study the thermal runaway of a wide range of ASSB technologies. We specifically designed a closed calorimeter to be used in operando experiments with high-speed synchrotron X-ray radiography for the validation of the principle.

Electrodes removed from LiB at 100 % state of charge have been reassembled in ASSB, with a LLZO (Lithium Lanthanum Zirconium Niobium Oxide) electrolyte. For the first time, we were able to observe and compare the thermal runaway of ASSB and liquid electrolyte (LiB) using this methodology. An 11 % decrease of heat release was measured in comparison with LiB during the thermal runaway. Such a methodology can assist in the development of future battery technologies, by evaluating battery safety from the start of the design from battery composition to cell shape.

Key words: Lithium-ion battery – Calorimeter – Thermal stability – Exothermic reaction – Heat released – Battery safety – All-solid-state – X-ray radiography

Introduction:

In the fight against global warming and reduction of carbon emissions to achieve a more sustainable and renewable energy, lithium-ion batteries (LiB) lead the way[1–3]. In this context, batteries autonomy needs to be increased. It requires cells with higher energy densities [4]. Nevertheless, battery safety is also a major concern[5,6]. Increasing density of active materials means also increasing thermal runaway (TR) hazard[7]. Devastating failures may occur as toxic smoke, fire and explosion[8–11]. To limit risks as well as to increase energy density, all-solid-state battery (ASSB) seems to be one of the most promising solution[12]. Unfortunately, as this technology is not mature yet, its safety has only been little studied[13].

Many dedicated devices increase the battery safety as management system, current interrupt device or vent[4,14]. However, there are still some failures, partly related to internal manufacturing defects[15]. The risk is extremely low but serious accidents still happen[8,16]. Hence, a proper characterization of the thermal runaway of new battery technologies is mandatory.

Liquid electrolyte LiB are studied a lot and account for 40 % of papers published on batteries in 2019[17]. Thermal runaway is an important subject of interest to make the batteries safer. The thermal runaway is characterized by an uncontrollable increase of cell temperature. However, the solid electrolyte interphase (SEI) film decomposition is the first reaction leading to thermal runaway[18]. During runaway, three temperatures are conventionally identified. The exothermic reaction starts with the cell self-heating when the onset temperature (T_{onset}) is reached[19]. The second specific temperature is the runaway initiation temperature (T_{ini}). The separator collapses and leads to internal short circuit[20–22]. Then, the maximum temperature (T_{max}) is reached[23]. A strong link exists between the maximum temperature and the heat release. For example, in the case of a Graphite | NMC811 ($LiNi_{0.8}Mn_{0.1}Co_{0.1}O_2$) battery, the onset, initiation and maximum temperatures reach respectively 85.57 °C, 157.54 °C and 858.22 °C[24].

Contrary to liquid electrolyte LiB, ASSB are less studied and account only for 3 % of the papers published on batteries in 2019[17]. It is generally accepted that ASSB are safer than liquid electrolyte LiB for the following reasons. Firstly, ASSB do not contain combustible organic electrolyte. Thus, the risk of combustion is expected to be very weak[25]. Secondly, between thermal initiation and thermal runaway, the main reactions are anode/electrolyte at 110 °C, electrolyte decomposition at 150 °C and cathode/electrolyte at 300 °C[18]. Thirdly, some ASSB have no interface between anode and solid electrolyte, i.e. they do not have SEI[2618]. Therefore, without liquid electrolyte and without SEI, it can be expected that ASSB are less likely to have a thermal runaway. *T. Inoue and K. Mukai* propose to define a degree of safety (DOS) from differential scanning calorimetry (DSC) analysis[27]. DOS is calculated from the ratio between thermal runaway enthalpies of ASSB and liquid electrolyte LiB. On their scale, a DOS of 100 % represents the safety of a liquid electrolyte LiB and a DOS of 0 % represents the ultimate safety. The ASSB with LLZNO (Lithium Lanthanum Zirconium Niobium Oxide) as solid electrolyte studied represent a DOS of 30 %[27]. Therefore, ASSB is presumed safer than liquid electrolyte LiB. *A. Bates* and al use thermodynamics models to show that solid electrolyte batteries could not be safer under short-circuit failure scenario [28]. That is why assess solid electrolyte batteries safety is a major concern.

But, thermal runaway mechanisms can be different between liquid electrolyte LiB and ASSB. For example, the T_{ini} is linked to short circuit and separator damage in liquid electrolyte LiB technology while for ASSB technology this temperature may indicate cathode destabilization thanks to ceramic stability at this temperature[29,30].

Nonetheless, as an immature technology, its safety has not been completely confirmed yet[31,32]. ASSB technology safety is difficult to assess. The currently developed cells have mainly low capacity (some mAh) and solid electrolyte to active materials ratio, which is a miss-representation of reality, and could lead to overestimate their safety.

Based on these observations, we have developed a specific methodology to investigate ASSB technology safety useful also for no-mature technologies. A fully charged

cell with same 3 Ah capacity and the same mass composition to ASSB ceramic technology was designed for this study from a commercial 18650-type cell (LGHG2, 3Ah). We modified the commercial cell to create an ASSB at a potential of 4.2 V and 100 % state of charge (SOC 100). This means without liquid electrolyte, salt and SEI and substituting polyethylene separator with a PEO-LLZO (Polyethylene oxide - Lithium Lanthanum Zirconium Oxide) composite solid electrolyte, chosen here for its better thermal stability. Our ASSB in a charged state is finally composed of graphite/silicon as anode material, PEO-LLZO as electrolyte, and NMC 811 as cathode material.

PEO-LLZO was chosen as solid electrolytes because LLZO is one of the most attractive solid electrolytes[32], thanks to its relatively high ion conductivity, a relatively good thermal stability and wide electrochemical window[33]. Moreover, LLZO electrolyte enables a stable cycling over 700 hours[34]. Furthermore, when LLZO is mixed with a polymer, it could enhance its mechanical properties and its thermal stability simultaneously while removing dendrite formation[35–37]. Therefore, this electrolyte composite seems relevant from the safety point of view. In addition to its high safety, ASSB using LLZO as electrolyte offer the same performance as conventional liquid LiB[38,39]. When preparing solid electrolyte, special care was taken to ensure a minimum of 85 % of LLZO by mass and a thickness in the 3 to 8 µm range[38,39].

As expected, due to the non-optimized electrode interfaces, the internal resistance of this ASSB is too high to perform electrochemical characterizations. Nevertheless, all present chemical materials are in correct form for TR assessments. In particular, the cells present an OCV (open circuit voltage) of 4.2 V between the electrodes in order to study their destabilization during TR.

Both liquid LiB and ASSB cells were overcoming an overheating of 6 °C/min ramp according to DO311 to assess their safety capabilities[40]. A heater wire was wound around the cell to comply with this instruction. In addition, the cell was equipped with two k-type thermocouple and voltage wires. The goal has been to compare induced risks by thermal

runaway of both cells by measuring TR initiation and maximum temperatures, the energy released, the kinetics, volumetric flow rate and the amount of gas. Furthermore, an in-situ look of the battery structure overcoming thermal runaway could potentially be of great interest.

Operando X-ray fast radiography, allows to assess and understand the internal structural behavior of a cell during TR[41]. X-ray radiography is a non-destructive technique that provide a high spatial resolution in two-dimension (2D) to perform such diagnostic[42]. Characterizing TR kinetics is challenging due to the TR event speed (within 1 second), in link with the evolution of internal structure as delamination, gas pockets, formation of projectiles[43–45] or the unpredictability of TR start location[46]. With an intense beam flux, synchrotron x-ray source enables high-speed radiography at high spatial resolution.

As specific setup, we developed a calorimeter to link external measurements (temperature, pressure or voltage) and X-ray radiography (Figure 1). The calorimeter was made of a stainless-steel tube; this closed system was thin enough to allow high energy X-rays to be transmitted through the top part of the cell and to contain overpressure and TR. The covered volume of the cell by the X-ray beam is 20 × 10 mm^2. External measurements of temperature and pressure sensors were recorded during the full extent of the protocol. High-speed X-ray radiography was performed at ID19 beamline of the European Synchrotron Radiation Facility (ESRF). The cells internal dynamics was observed by recording X-ray radiographs at 2000 frames per second (fps) for 12 seconds. We chose X-ray radiography to have an inside observation of the TR and visualized the differences in cell behavior.

External measurements and internal structure of liquid LiB and ASSB cells were compared to demonstrate the gains and safety limits of ASSB. Moreover, this calorimeter allows to link external measurements like volumetric flow rate with the cell internal structure.

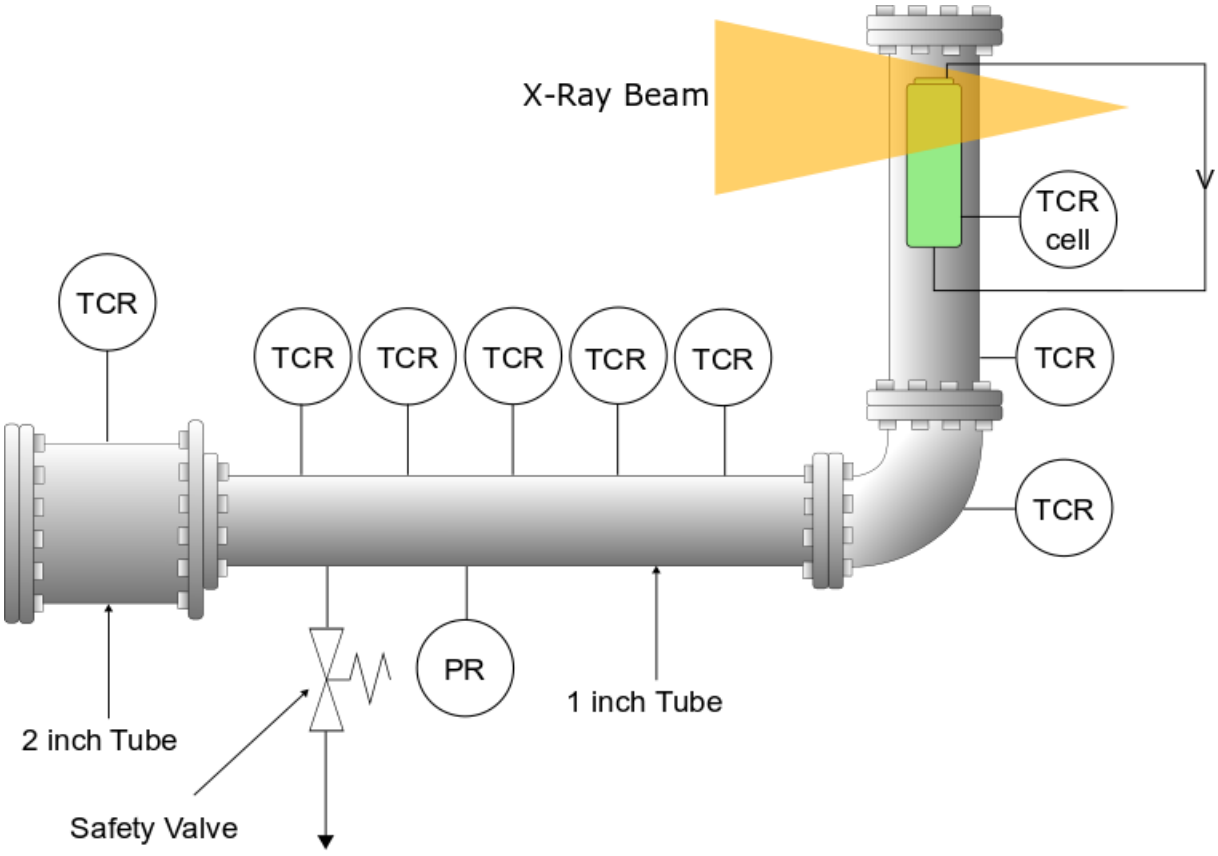

Figure 1: Plan of the calorimeter and instrumented cell crossed by the X-ray beam with thermocouples recording (TCR) and pressure recording (PR).

Results:

Thermal runaway parameters:

Thanks to the calorimeter design described in the introduction section, various measurements were possible during thermal runaway of liquid-electrolyte LiB and ASSB. Moreover, our calorimeter only recorded external measurements by the various sensors like battery surface temperature and gas pressure at the cell closest vicinity during TR. These physical quantities are plotted in Figure 2Figure 2 for the liquid-electrolyte LiB and solid-electrolyte cell. Firstly, during the phase A, until the TR initiation temperature (T_{ini}) at t_{ini}, the temperature increases linearly in agreement with the heating system (about 6 °C per minute) with no evolution of the pressure. Then, during the phase B, the pressure and temperature surge up to P_{max} and T_{max}. Lastly, during phase C, the pressure declines drastically until a

balancing pressure (P_b) and temperature decreases slowly up to ambient temperature (T_{amb}). The three stages seem similar regardless of the technology. Subsequently, the phase of thermal runaway was studied more specifically.

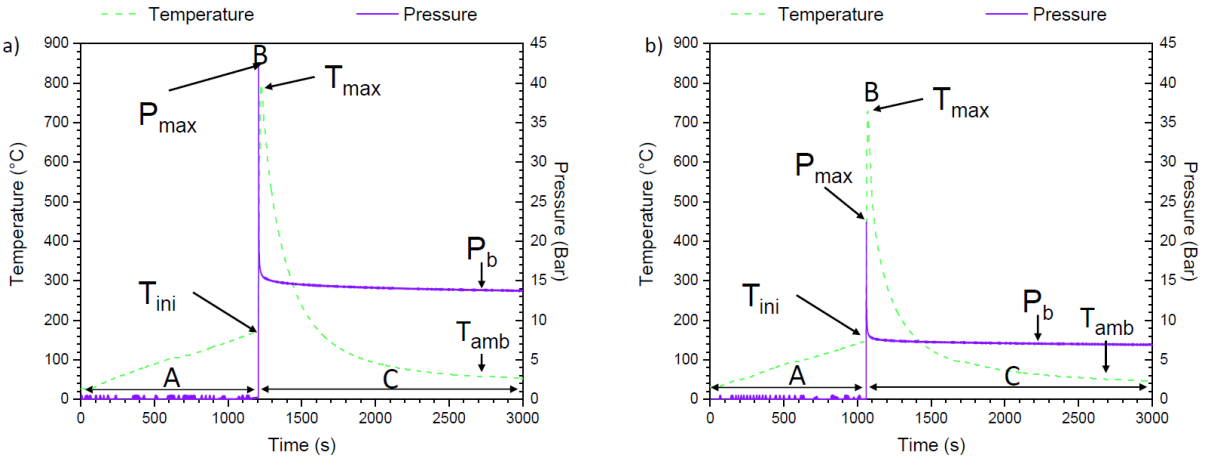

Figure 2:a) Liquid-electrolyte LIB and b) solid-electrolyte cell at SOC 100 time course of the battery surface temperature and pressure in the calorimeter with phase A, temperature ramp of 6°C/min, phase B, thermal runaway of the cell and phase C, cooling of the cell

We can show Figure 2 that the time course of thermal runaway seems similar. The major difference is maximal pressure. It is twice as large for the liquid-electrolyte cell.

Cell observation by X-ray radiography:

TR occurs during phase B, around pressure and temperature peaks (Figure 2 phase B). It is analyzed using high-speed X-ray radiography to observe the cell internal reactions. This imaging technique allows comparing the thermal runaway of liquid-electrolyte LiB and ASSB. Only a sub volume of the cell is imaged as shown in Figure 1. To our knowledge, it is the first time the internal reactions during ASSB thermal runaway are observed, unlike LiB case with its exhaustive literature. Figure 3 and Figure 4 show respectively three sequences during the runaways of a LiB cell and of an ASSB cell. These sequences are extracted from the full recording of the thermal runaways of the cells given in the supplementary movie 1 – Part A and supplementary movie 2 – Part A.

For liquid-electrolyte LiB, the first reaction show a jelly-roll collapse at t_{ini+}75ms. First, gas pockets appear with an electrode assembly delamination at $t_{ini+120ms}$.At $t_{ini+165ms}$ the first particle is evacuated (Figure 3b). At $t_{ini+235ms}$, $t_{ini+325ms}$, $t_{ini+450ms}$ and $t_{ini+500ms}$ particles and gas are ejected in waves. The delamination of electrodes occurs from the center to the periphery (Figure 3 b and c). ASSB cell displays a different behavior. The first particle is evacuated at $t_{ini+80ms}$. Electrode's delamination starts at $t_{ini+130ms}$, from center to the periphery. At $t_{ini+200ms}$, the jelly roll moves in the packaging. At $t_{ini+390ms}$, particles and gas are ejected in one wave (Figure 4b). This wave trigger a large mechanical force turning off the positive pole turn at $t_{ini+440ms}$ (Figure 4c)

Figure 5 and Figure 6 show a schematic illustration of the observed phenomena for liquid-electrolyte LiB and ASSB respectively. In the two cases, these drawings show the evacuation of the first particle, the particles and gas ejection in waves, the delamination of electrodes layers occurring from the center outwards, and the decomposition of the electrochemical assembly layers (anode, separator and cathode), one after the other. The reaction occurs from the center to the outer layers because of the self-heat of both cells. From the regulation of the heating wire, a self-heating starts from 120 °C for both technologies. Despite the influence of the heating wire, as the heat losses occur at the periphery of the battery, the self-heating generates a higher temperature at the core of the cell. Visually, there is no difference between the thermal runaway of liquid-electrolyte LiB and that of ASSB. Furthermore, the reaction kinetic appears to be faster for ASSB than for liquid-electrolyte LiB.

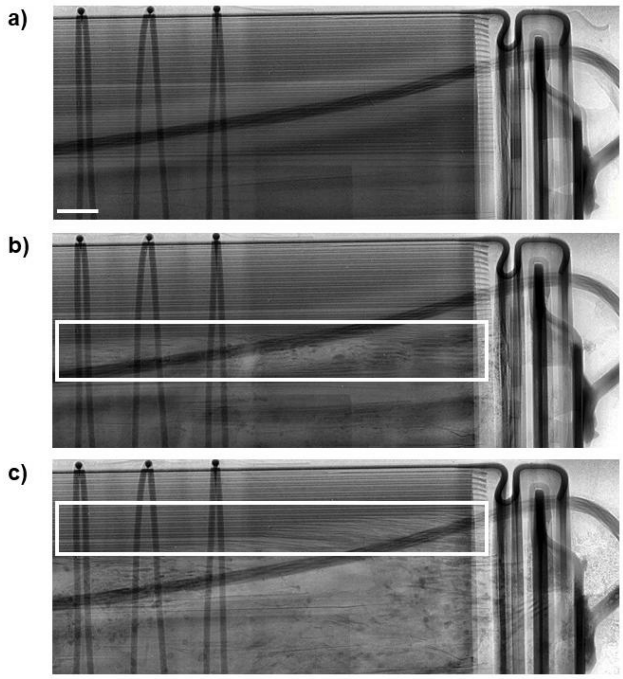

Figure 3 :X-ray radiographies during the thermal runaway (Figure 2 phase B) of a liquid-electrolyte LiB cell at SOC 100 at (a) t_{ini},, (b) $t_{ini+165ms}$ where the white rectangle indicates the area of the active material reacting between $t_{ini+165ms}$ and $t_{ini+235ms}$), and (c) $t_{ini+325ms}$ where the white rectangle indicates the active material reacting between $t_{ini+325-ms}$ and $t_{ini+370ms}$. The white bar gives the 2 mm scale.

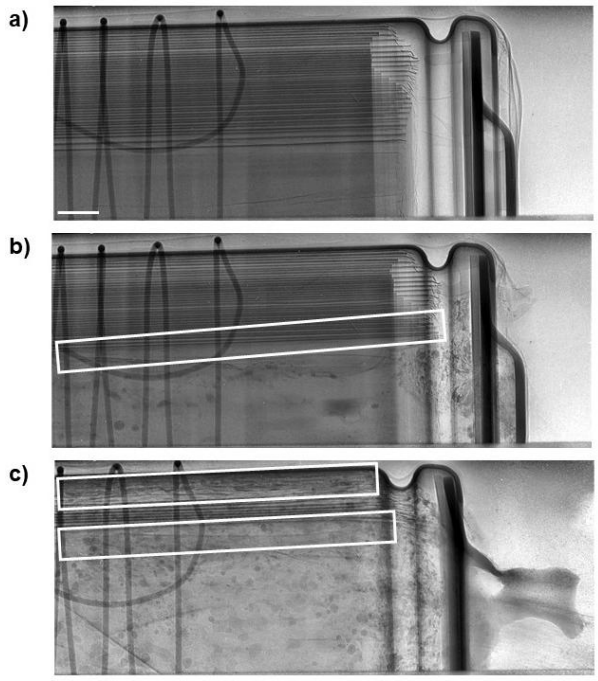

Figure 4: X-ray radiographies during the thermal runaway (Figure 2 phase B) of an ASSB cell at SOC 100 at (a) t_{ini}, (b) $t_{ini+335ms}$ where the white rectangle indicates the area of the active material reacting

between $t_{ini+335-ms}$ and $t_{ini+380ms}$, and (c) $t_{ini+465ms}$ where the white rectangle indicates the area of the active material reacting between $t_{ini+465ms}$ and $t_{ini+480ms}$. The white bar gives the 2 mm scale.

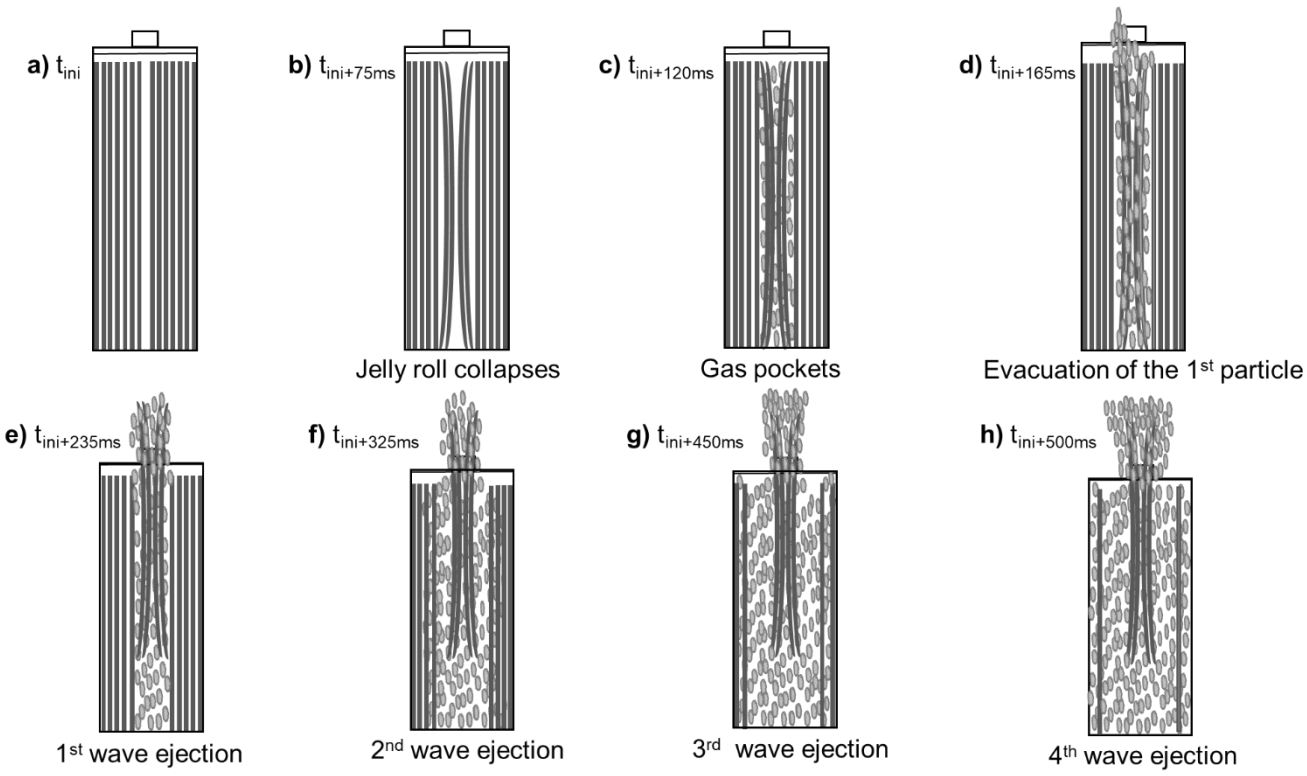

Figure 5 : Drawings of the internal behavior of a liquid-electrolyte cell during a thermal runaway at SOC 100 (Figure 2 phase B) were the grey rectangles represent the electrochemical assembly layer (graphite/silicon + PE + NMC811) and the grey clouds represent particle aggregates with (a) cell before thermal runaway, (b) jelly roll collapse, c) formation of gas pockets, (d) evacuation of the first particles and (e-h) particles and gas wave ejections. Supplementary movie 1 - Part A shows the corresponding internal behavior.

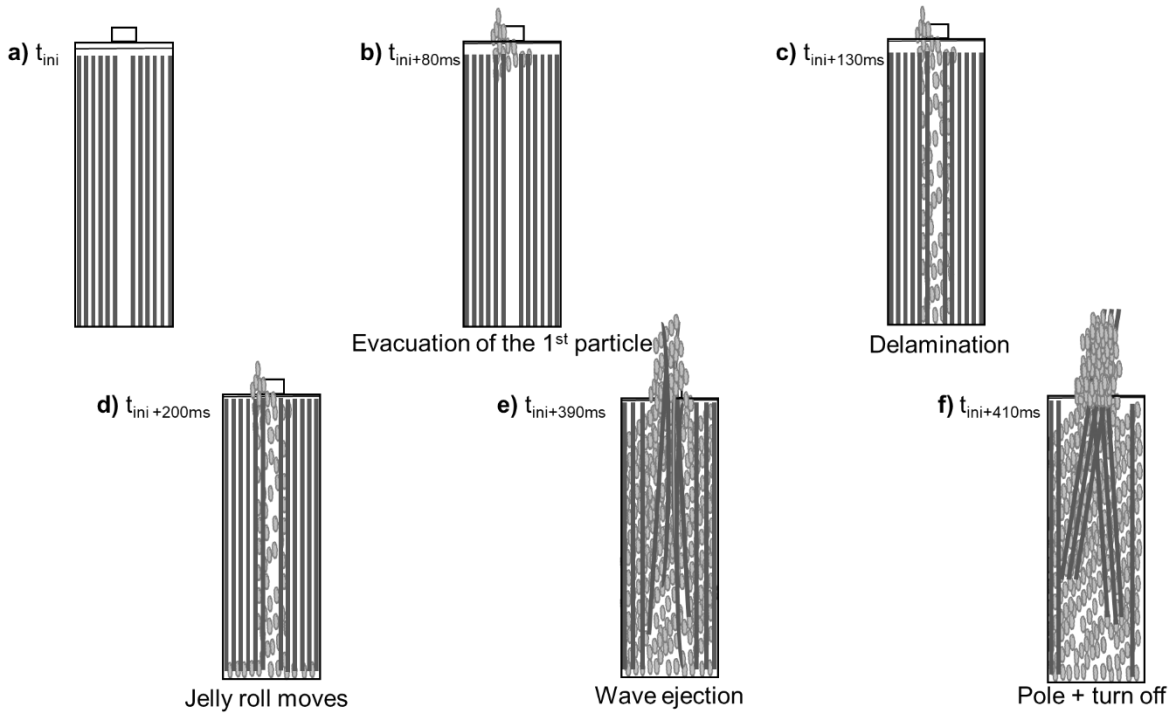

Figure 6 : Drawings of internal behaviors of an ASSB cell during a thermal runaway at SOC 100 (Figure 2 phase B) were the grey rectangles represent the electrochemical assembly layer (graphite/silicon + PEO/LLZO + NMC811) and the grey clouds represent particle aggregates with (a) cell before TR,(b) evacuation of the first particle (c) delamination, (d) jelly roll motion, (e) particles and gas wave ejections and (f) positive pole turn off. Supplementary movie 2 - Part A shows the corresponding internal behavior.

Quantitative analyses:

We compute the percentage of reactive materials from the X-ray radiographies. Despite a partial analysis of the cell by the X-ray radiography (Figure 1), a symmetrical reaction through the full cell volume is assumed as seen in Figure 5 and Figure 6 . We calculate the percentage $rm\%$ by volume of reactive materials at t_0 from Eq.1

$$rm\% = \frac{L_{LR}}{L_{tot}} * 100 \ \#(1)$$

where L_{tot} is the total length of the electrode layer (m) and L_{LR}, the length of electrode layer having reacted whenever one or more layers are delaminated (m). The length of the electrode is calculated from the perimeter defined by its position as a function of the radius.

Figure 7 shows the time course of the volume of gas, the volumetric flow rate and the amount of reactive material during the thermal runaway for the two kinds of cells. The filled circle marks represent the experimental percentage of the reacted material versus time as calculated from the supplementary movie 1- Part B and supplementary movie 2 – Part B. The arrows correspond to the images shown in Figure 3 and Figure 4. At t_{ini}, when none of the electrode layers has reacted yet for both designs, the total electrode length L_{tot} is 911 mm and 847 mm for the liquid-electrolyte LiB cell and the ASSB cell respectively (Figure *3*a and Figure 4a). For the liquid-electrolyte LiB cell (Figure 7a), the length L_{LR} of the electrode layer having reacted at $t_{ini+165ms}$ and $t_{ini+325ms}$ is, respectively 71 and 289 mm (Figure *3*b and Figure *3*c). This corresponds to a percentage $rm\%$ of reactive materials of 8 and 32 % by volume respectively. For the ASSB cell (Figure 7b), the length L_{LR} of the electrode layer having reacted from the cell center at $t_{ini+335ms}$ and $t_{ini+465ms}$ (Figure 4b and Figure 4 c) is, respectively, 97 and 587 mm i.e. $rm\%$ values of 11 and 69 % by volume.

In addition, we have recorded thermal runaway parameters such as pressure or temperature provided by calorimeter sensors. It allows correlating the cell internal reaction with external measurements. From the pressure measurements, we calculate the instantaneous volume V (m^3) of gas released during thermal runaway using Eq.2

$$V = \frac{V_{cal} * P}{P_{atm}} \#(2)$$

where P is the instantaneous internal pressure (Pa), V_{cal}, the calorimeter volume (m^3) and P_{atm}, the atmospheric pressure (Pa). Then we calculate the volumetric flow rate $\dot{V}$ ($m^3.s^{-1}$) using Eq.3

$$\dot{V} = \frac{\Delta V}{\Delta t} \#(3)$$

where ΔV (m_3) is the volume variation during the time period Δt (s). The volumetric flow rate curves are plotted as a function of time (Figure 7 and supplementary movie 1 – Part C and

supplementary movie 2 – Part C).

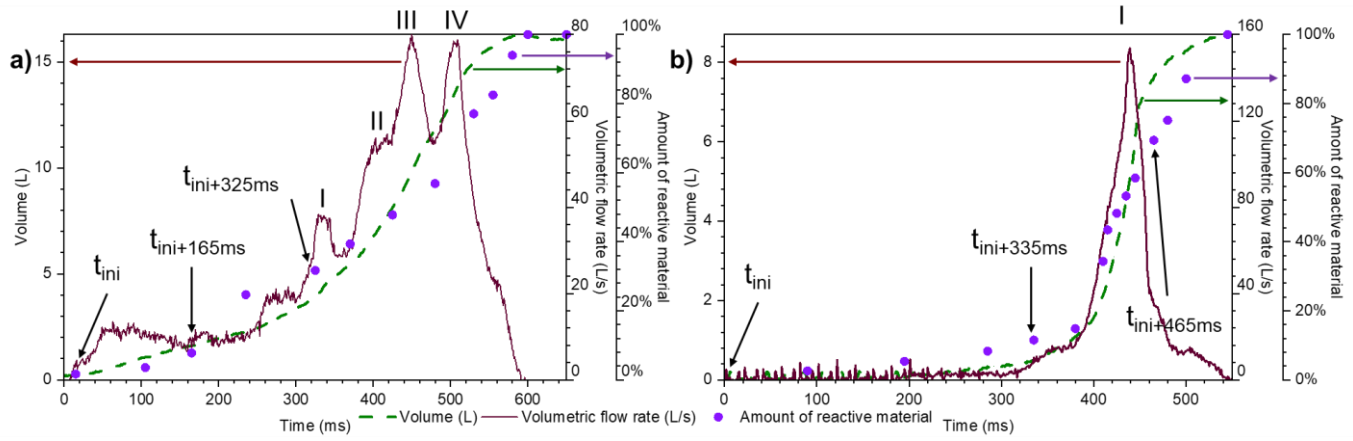

Figure 7 : Time course of the volume of gas (solid line), the volumetric flow rate (dash line) and the amount of reactive material (filled circle marks) during the thermal runaway (Figure 2 phase B) for (a) the liquid-electrolyte Li-ion cell at SOC 100 where and peaks LiB-I, LiB-II, LiB-III and LiB-IV correspond to the forth ejections in Figure 5e, f, g and h, respectively and (b) the solid electrolyte cell at SOC 100 where the peak ASSB-I correspond to the ejection in Figure 6e.

The volumetric flow rate time course of the liquid-electrolyte LiB cell (Figure 7a) and the ASSB cell (Figure 7) show a fast increase with respectively four maxima and one maxima. We relate these behaviors to an increase of internal reactions speed and dust quantity released during TR as shown on supplementary movies. The strong correlation between radiographies and flow measurements gives valuable insight worth further investigation of the sensors data. Moreover, it is interesting to notice that a strong interdependence between the estimated percentage of reacted active materials and the ejected gas volume measured by pressure sensor is observed. It indicates that TR occurs from local chemical reactions, propagating radially from the center. Furthermore, the duration of thermal runaway is about 200 ms for solid electrolyte cell i.e. about twice as long as liquid electrolyte cell.

In addition, we carried out several tests with the same calorimeter by adding an insulated box to assess the safety of different battery technologies. In Table 1, we compare

the TR data, averaged on four cells, of the temperature T_{ini} at TR initiation, the maximum reached temperature T_{max}, the heat release Q_+, the gas quantity n_{gas} and the duration d_{TR} of TR. We compute the heat release Q_+ (kJ) from the calorimeter enthalpy using Eq. 4.

$$Q_+ = m_{cal}.c_{p\_cal}.\Delta T_{cal} - Q_{heating} \#(4)$$

Where, m_{cal} is the mass of the calorimeter (kg), c_{p_cal} is the mean specific heat capacity of the calorimeter ($kJ.kg^{-1}.K^{-1}$), ΔT_{cal} is the temperature change of the calorimeter (K) and $Q_{heating}$, the heating energy applied to the cell (kJ).

The amount of substance n_{gas} (mmol) is obtained from the ideal gas law using Eq.5.

$$n_{gas} = \frac{P_s.V_{cal}}{\mathrm{R}.T_s} \#(5)$$

Where P_s is the stable pressure (Pa), T_s is the stable temperature (K), V_{cal} is the calorimeter volume (m^3), R the ideal gas constant ($J.K^{-1}.mol^{-1}$).

We take as the duration d_{TR} of TR, the period of time between 5 and 95 % of the total gas production to eliminate the uncertainties associated with phases delay.

Cell kind	T_{ini} (°C)	T_{max} (°C)	Q_+ (kJ)	n_{gas} (mmol)	d_{TR} (ms)
Liquid-electrolyte LiB	159 ± 10	821 ± 90	78.5 ± 3.0	262 ± 15	329 ± 60
ASSB	148 ± 6	813 ± 134	69.8 ± 3.4	156 ± 31	191 ± 42

Table 1 : Data of TR averaged on four cells for liquid-electrolyte LiB cells and ASSB cells at SOC 100

There is no difference between TR initiation temperatures (T_{ini}) of liquid-electrolyte LiB cells and ASSB cells. Therefore, there is no additional mechanism when triggering TR for ASSB cells compared to liquid-electrolyte LiB ones. Moreover, NMC811 destabilization temperature is 157 °C which correspond to liquid-electrolyte LiB cell T_{ini}[24]. The maximum temperature recorded for both technologies are about 820 °C. The interaction between the electrodes makes it possible to reach the maximum temperature. The values for the liquid-

electrolyte LiB are in line with the ones reported by *Wang et al*[24]. The duration of thermal runaway for solid electrolyte cell is about twice as fast as the liquid electrolyte cell.

The energy released for the liquid-electrolyte LiB cells is 78.5 ± 3.0 kJ, showing a standard deviation in agreement with *Walker et al*[47]. Figure 8 shows the normal distribution curves based on the observed thermal runway energy released by both cell technologies. The energies released from the liquid-electrolyte LiB cells and the ASSB cells represent two distinct populations.

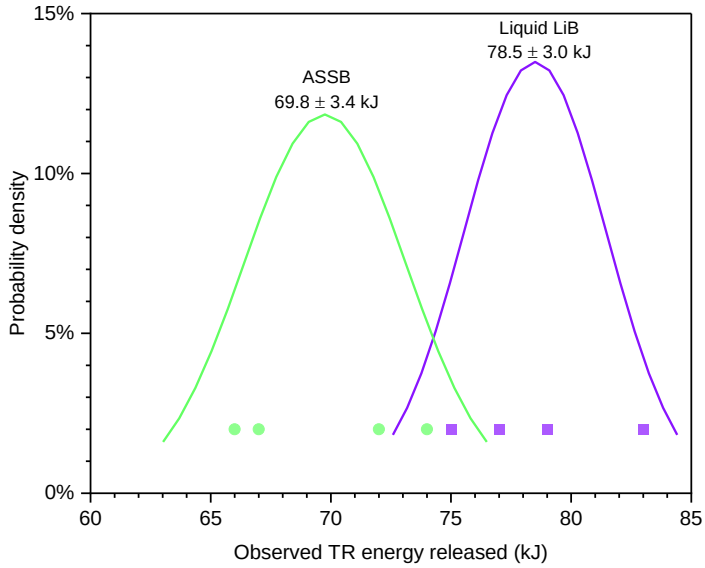

Figure 8 : Normal distribution curves based on the observed thermal runway energy released with the energy released by (circles) the ASSB cells and (squares) the liquid-electrolyte cells for each of the four tests at SOC 100

The energy released by the ASSB cells is weaker than the one released by the liquid-electrolyte LiB cells by about 11 % (Table 1). Standard deviations show similar magnitude for the two technologies demonstrating the replicability of our ASSB manufacturing. The SEI films can not be perfectly removed by washing with DMC [48] however most of the SEI is removed. Moreover, the quantities of material have a major role in thermal runaway reactions unlike interphases. Therefore, the impact of the SEI residues could be neglected. Of course,

the energy of a battery could be somewhat lower for various reasons (interphases, residual SEI films and additional PEO), but it reflects the impact of the quantities of material on the energy released during TR. The difference in energy release could be explained by the lower lithium mass in ASSB technologies due to the absence of SEI and of salt caused by the electrode washing with DMC[49,50]. As quoted by *Wang et al*[7], this could induce that the following chemical reaction given by Eq.6 cannot take place even if the irreversible SEI represent about 10 % of lithium and can react during TR.

$$(CH_2OCO_2Li)_2 \rightarrow Li_2CO_3 + C_2H_4 + CO_2 + \frac{1}{2}O_2 \ \#(6)$$

Moreover, in this technology, lithium cannot react with oxygen and form compounds as $LiAlO_2$, Li_2O or Li_2CO_3[51].

The quantity of gas is 40 % higher for the liquid-electrolyte LiB cells than for the ASSB cells. Contrary to the ASSB technology, liquid-electrolyte LiB has a larger amount of organic components (electrolyte and separator), which degrade during TR. Therefore, more gas is released. Moreover, we observe the kinetics is 42 % faster for the ASSB cells than for the liquid-electrolyte LiB. A significant decrease of organic products (electrolyte, separator) and salt could allow a better heat transfer through electrodes. That certainly explains for the faster TR kinetics in the ASSB technology, which is twice as swifter as liquid LiB technology. In addition, electrolyte evaporation may be a brake on TR.

Discussion:

Thanks to the calorimeter and X-ray radiography, we were able to visualize and compare the thermal runaway (TR) of a liquid-electrolyte LiB and ASSB. First, we have shown a direct correlation between the amount of matter reacting in the cell and the volume of gas released at each stage of the thermal runaway. Secondly, we were able to qualitatively relate the transient phenomenon in the cell (the flow of dust ejected) and the gas flow peaks calculated from the pressure derivative. To our knowledge, it is the first time in the

field that, a direct link between the pressure measurement in the calorimeter and the reactions inside the cell during the TR is demonstrated.

These results are particularly important for the security management of the ASSB cells. On the one hand, it could optimize the design of the cell casing and of the vent to limit the obstruction risk and the unscrewing of the cells. On the other hand, the link between the reaction of a small amount of material and externally measurable parameters during TR allows working on a specific design of representative small cells to support the modeling of the reaction kinetics of large cells (> 100 Ah). In addition, from the reaction speed in the different planes of the cell (along and through the electrodes), it is now possible to predict the behavior of all cell shapes.

At the same time, we have developed a methodology to make ASSB cells that TR consequences are representative of 100 %-charged cells from ASSB technologies. The reconstitution of an ASSB cell, non-fully electrochemical effective but composed of an LLZO electrolyte with charged electrodes, allows us to measure a trend to a small decrease (11 ± 10 %) in the released energy during TR for the ASSB cells compared to the liquid-electrolyte LiB cells which could reduce the risk of propagation. In addition, the amount of gas released decreased significantly by 40 ± 20 % for the ASSB cells compared to the liquid-electrolyte LiB cells which could reduce the amount of toxic gases and decrease the risk of ATEX (explosive atmospheres). However, the reaction kinetics increased by 42 ± 20 %, which should be studied further to design safer new cell generation. The confidence intervals are given at 95 %.

The decreases of energy release on ASSB cells can be explained by the reduction of combustible quantity in the cell as the electrolyte, the separator, the SEI and the salt. However, it is important to emphasise that the decrease of released energy is not sufficient to avoid the TR propagation to other cells. In addition, the thermal degradation of the electrolyte and the separator into a shorter organic molecule can largely explain the greater

amount of gas for liquid-electrolyte LiB cells. In a future study, the analysis of runaway gases and dust will allow us to deepen these assumptions.

Conversely, the higher reaction kinetics of the ASSB cells are certainly due to a better thermal conduction of ceramics compared to the separator or to the evaporation of a part of electrolyte in the liquid-electrolyte LIB cell. For the design of larger cells, the increase in ASSB reaction kinetics is an important key parameter with a potentially very high volumetric flow rate (> 10000 L/s). Thus, an incorrect design of the pack casing could result in a fatal rupture.

There is numerous ASSB cells with different chemistries, as ceramics (LLZO, LATP), glasses (sulfide, argyrodite), polymers (PEO, PCL) and hybrid materials (PEO + LLZO). Here, based on the stable PEO/LLZO solution with standard charged electrodes NMC 811| graphite/silicon, TR runaway is observed with over temperature. At this stage, we show that these technologies are not completely safe.

Conclusion:

For the first time, in situ synchrotron X-ray radiography were used to visualise solid electrolyte batteries during thermal runaway. It is also the first time that calorimetric and morphological change are studied together.

We show that solid electrolyte batteries could no be safer than liquid electrolyte batteries. Solid electrolyte batteries should be continue to be challenged.

In the future, thanks to this proposed methodology, it should be possible to guide the development of new battery technologies, evaluating from the start of the design, the safety of the cell through heat and gas released according to its composition and format.

Experimental procedures:

Calorimeter

Calorimeter is a closed system thermally insulating and the access to air is limited. Made of a 25.4 mm diameter stainless steel tube thin enough to allow X-rays transition and large enough to fit a cell (Figure 1). Moreover, this calorimeter allows containing overpressure and TR. A 50.8 mm diameter stainless steel tube is used to increase calorimeter volume and prevent the risk of overpressure. In the unlikely event of overpressure, a 180 bar safety valve is integrated. That calorimeter allows, to measure energy release by placing it in an insulated box.

The cell is wounded with a heating wire of 0.32 mm diameter. The cell-heating wire is connected to a power supply allowing to heat the cell uniformly with a 6 °C per minute temperature ramp. To isolate electrically the cell from its holder, a polytetrafluoroethylene (PTFE) tape is used. Voltage sensors are welded to the cell and give a measurement every 500 ms. Nine type-k thermocouples are placed on the calorimeter to measure the stainless steel tube temperature at different locations. Two type-k thermocouples are placed in the middle of the cell to measure the cell surface temperature (Figure 1). The Sensors temperature is acquired every 500 ms. A 100-bar range pressure sensor is used to measure the pressure every 1 ms in the cell closest vicinity during TR.

ASSB preparation

A commercial 18650-type cell from LG (LGHG2) is discharged at a state of charge of 0 % (SOC 0). The following operations are done under an argon atmosphere in a glove box with an oxygen and water rate lower than 0.1 $mg \cdot L^{-1}$. The negative pole of the cell is drilled with a drill bit of 0.6 mm. Then the cell is charged at a SOC 100 as liquid electrolyte cells i.e 1.5 A charged to 4.2 V with 50 mA End-current (CC-CV). The electrolyte is evaporated under vacuum and at 70 °C temperature for 24 h. This process consists on drying the cell to eliminate the entire liquid electrolyte and avoid component deterioration. To ensure full

evaporation, the cell resistance is continuously measured. The electrodes are removed from the casing and separated. The electrodes are washed twice during 3 min in DMC and then, they are dried under vacuum for 4 h. The electrode washing with EC/PC/3DMC allows to remove SEI lithium compounds like Li_2CO_3, LiOH, Li_2O, $LiOCH_3$ and $LiOC_2H_5$[49]. Moreover, the anode washing with DMC allows to remove $LiPF_6$ salt and SEI lithium compounds as LiF and Li_xPF_y[50]. Even if DMC remove SEI, a new SEI film could be formed [48]. However, its amount of material could be neglected. The positive electrode is coated by LLZO mixture in anhydrous room. This positive electrode is wounded with the negative one inside the glove box and the whole is put in an 18650-type cell casing. The ASSB cell, charged at SOC 100-, is finally crimped with the venting and the positive pole in anhydrous room.

The LLZO slurry composed of 21 % of LLZO (Nanomyte® from NEI Corporation), 4 % of PEO (300 000 g/mol from Sigma-Aldrich) and 75 % of acetonitrile (99.8 % anhydrous from Sigma-Aldrich) is prepared at room temperature in a anhydrous room (dew point at -40 °C) by using a dispersing device (Dispermat® LC). LLZO and PEO is beforehand dried at 55 °C for 48 h. The mixture is intensively grind-mixed for at least 10 min. This slurry is then coated on the cathode by using an automatic film applicator from Elcometer® (Elcometer 4340) with a gap size of 40 µm. The film is dried overnight under extractor fan at room temperature for 12 h.

Beamline description

High-speed X-ray imaging of the cells is performed at the ID19 beamline of the ESRF facility. A polychromatic X-ray beam at a peak energy of 114 keV is used to cross the chamber of 4 mm stainless steel with the cell. Synchrotron X-ray source are particularly suited to provide high photon flux allowing for 2000 image·s^{1} for 12 s with a PCO-Dimax ® detector (PCO AG, Germany) and a 1000 µm LuAG(Ce) ($Lu_3Al_5O_{12}$:Ce) scintillator. The 11 µm detector pixel size was coupled to a magnification system giving an effective image pixel size of 22 µm and a field of view of 1273 × 507 pixel^2 or 28 × 1 mm^2 (Horizontal x Vertical). All acquired images were flat field corrected.

Data processing

The x-ray radiography movies are analyzed using ImageJ 1.53. The function, image calculator divide is used to divide selection by the specified real constant. It helps to remove imperfections related to the camera and to the stainless steel tube. Two functions –enhance contrast and enhance local contrast– help to optimize brightness and contrast. 32-bit images are compiled into movies with “avi” file extension. OpenShot Video Editor 2.4.4 is used to edit movies and to show the links between radiographies and volumetric flow rate or reactive materials.

Acknowledge

The authors would like thanks Jérôme Cognard, David Brun-Buisson, Kamel Bachir Elezaar and Pierre Balfet for technical assistance and technical discussion regarding to abuse tests. The authors thanks also Christophe Vincens for technical assistance regarding to all-solid-state manufacturing.

We are grateful for the provision of synchrotron beamtime by the ESRF on beamline ID19 and for allowing us to use their facilities (proposal no. MA4622). A part of this work has been also operated by the Grenoble Battery Hub under Long Term Project « Multi-scale Multi-techniques investigations of Li-ion batteries: towards a European Battery Hub » (pilot proposal no. MA4929).

The authors would like to acknowledge the financial support from the European Union under the Horizon 2020 research and innovation program (TEESMAT project grant agreement No. 814106) for the setup development by CEA.

Author contributions

R.V conceived the work. J.C, R.V and C.D carried out the fabrication of all-solid-state cells. J.C and N.D performed the abusive tested. J.C, N.D, C.D, L.B and R.V performed X-ray radiographies. J.C, N.D, C.D, L.B and R.V wrote the original draft. J.C, N.D, C.D, L.B, M.R, PXT and R.V discussed the results, critically reviewed and revised on the manuscript.

Competing interest statement

The authors declare no competing interests

Supporting Information:

Supplementary movie 1 (High-speed radiography video showing the thermal runaway of a LGHG2 cell. The part A shows the different steps leading to thermal runaway. The part B establish a link between the volume of gas released and the amount of material reacting. The part C make a connection between volumetric flow rate peaks and the moments where particles and gas are ejected.)

Supplementary movie 2 (High-speed radiography video showing the thermal runaway of an all-solid-state cell (Graphite-LLZO-NMC). The part A shows the different steps leading to thermal runaway. The part B establish a link between the volume of gas released and the amount of material reacting. The part C make a connection between volumetric flow rate peaks and the moments where particles and gas are ejected.)

References

(1) Di Lecce, D.; Verrelli, R.; Hassoun, J. LithiumionBatteries sustainable energy storage: recent advancesNewcellConfigurations. *Green Chem.* **2017**, *19* (15), 3442–3467. https://doi.org/10.1039/C7GC01328K.

(2) Armand, M.; Tarascon, J.-M. BuildingBetterBatteries. *Nature* **2008**, *451*, 652–7. https://doi.org/10.1038/451652a.

(3) Larcher, D.; Tarascon, J.-M. TowardsGreener More Sustainable BatteriesElectricalEnergyStorage. *Nature chemistry* **2015**, *7*, 19–29. https://doi.org/10.1038/nchem.2085.

(4) Doughty, D.; Roth, E. AGeneralDiscussion Li Ion Battery Safety. *Electrochemical Society Interface* **2012**, *21*, 37–44. https://doi.org/10.1149/2.F03122if.

(5) Goodenough, J. B. Evolution StrategiesModernRechargeableBatteries. *Accounts of Chemical Research* **2013**, *46* (5), 1053–1061. https://doi.org/10.1021/ar2002705.

(6) Wu, H.; Zhuo, D.; Kong, D.; Cui, Y. ImprovingbatterySafety early detectionInternalshorting bifunctional separator. *Nature communications* **2014**, *5*, 5193. https://doi.org/10.1038/ncomms6193.

(7) Wang, Q.; Mao, B.; Stoliarov, S. I.; Sun, J. Areview lithium ion battery failure mechanismsFirepreventionStrategies. *Progress in Energy and Combustion Science* **2019**, *73*, 95–131. https://doi.org/https://doi.org/10.1016/j.pecs.2019.03.002.

(8) Zalosh, R.; Gandhi, P.; Barowy, A. LithiumionEnergystorageBatteryexplosionIncidents. *Journal of Loss Prevention in the Process Industries* **2021**, *72*, 104560. https://doi.org/https://doi.org/10.1016/j.jlp.2021.104560.

(9) Baird, A. R.; Archibald, E. J.; Marr, K. C.; Ezekoye, O. A. Explosionhazards lithium-ion battery vent gas. *Journal of Power Sources* **2020**, *446*, 227257. https://doi.org/https://doi.org/10.1016/j.jpowsour.2019.227257.

(10) Golubkov, A. W.; Planteu, R.; Krohn, P.; Rasch, B.; Brunnsteiner, B.; Thaler, A.; Hacker, V. Thermalrunaway large automotive Li-ion batteries. *RSC Adv.* **2018**, *8* (70), 40172–40186. https://doi.org/10.1039/C8RA06458J.

(11) Sun, P.; Bisschop, R.; Niu, H.; Huang, X. AReview Battery FiresElectricVehicles. *Fire Technology* **2020**, 1–50. https://doi.org/10.1007/s10694-019-00944-3.

(12) Fan, L.; Wei, S.; Li, S.; Li, Q.; Lu, Y. RecentProgress Solid-State ElectrolytesHighEnergyMetalBasedBatteries. *Advanced Energy Materials* **2018**, *8* (11), 1702657. https://doi.org/https://doi.org/10.1002/aenm.201702657.

(13) Wu, Y.; Wang, S.; Li, H.; Chen, L.; Wu, F. Progress thermal stabilityAllsolidStateLiIonbatteries. *InfoMat* **2021**, *3* (8), 827–853. https://doi.org/https://doi.org/10.1002/inf2.12224.

(14) Xu, B.; Lee, J.; Kwon, D.; Kong, L.; Pecht, M. Mitigationstrategies Li-ion battery thermal runaway: A review. *Renewable and Sustainable Energy Reviews* **2021**, *150*, 111437. https://doi.org/https://doi.org/10.1016/j.rser.2021.111437.

(15) Feng, X.; Ouyang, M.; Liu, X.; Lu, L.; Xia, Y.; He, X. ThermalrunawayMechanism lithium ion batteryElectricvehiclesAreview. *Energy Storage Materials* **2018**, *10*, 246–267. https://doi.org/https://doi.org/10.1016/j.ensm.2017.05.013.

(16) Williard, N.; He, W.; Hendricks, C.; Pecht, M. LessonsLearned 787 Dreamliner IssueLithiumIonBatteryReliability. *Energies* **2013**, *6* (9), 4682–4695. https://doi.org/10.3390/en6094682.

(17) Ma, J.; Li, Y.; Grundish, N. S.; Goodenough, J. B.; Chen, Y.; Guo, L.; Peng, Z.; Qi, X.; Yang, F.; Qie, L.; Wang, C.-A.; Huang, B.; Huang, Z.; Chen, L.; Su, D.; Wang, G.; Peng, X.; Chen, Z.; Yang, J.; He, S.; Zhang, X.; Yu, H.; Fu, C.; Jiang, M.; Deng, W.; Sun, C.-F.; Pan, Q.; Tang, Y.; Li, X.; Ji, X.; Wan, F.; Niu, Z.; Lian, F.; Wang, C.; Wallace, G. G.; Fan, M.; Meng, Q.; Xin, S.; Guo, Y.-G.; Wan, L.-J. The2021BatterytechnologyRoadmap. *Journal of Physics D: Applied Physics* **2021**, *54* (18), 183001. https://doi.org/10.1088/1361-6463/abd353.

(18) Tian, X.; Yi, Y.; Fang, B.; Yang, P.; Wang, T.; Liu, P.; Qu, L.; Li, M.; Zhang, S. DesignStrategies Safe ElectrolytesPreventingThermalRunaway Lithium Ion Batteries. *Chemistry of Materials* **2020**, *32* (23), 9821–9848. https://doi.org/10.1021/acs.chemmater.0c02428.

(19) Mao, B.; Huang, P.; Chen, H.; Wang, Q.; Sun, J. SelfheatingReaction thermal runaway criticalityLithiumionBattery. *International Journal of Heat and Mass Transfer* **2020**, *149*, 119178. https://doi.org/https://doi.org/10.1016/j.ijheatmasstransfer.2019.119178.

(20) Kim, J.-S.; Lee, D.; Lee, J.; Kim, C.-W. Optimization Lithium-Ion Battery Pouch CellMaximization Energy Density while Preventing Internal Short Circuit CausedSeparatorFailure Crush Load. *Journal of The Electrochemical Society* **2021**, *168*, 030536.

(21) Ren, D.; Feng, X.; Liu, L.; Hsu, H.; Lu, L.; Wang, L.; He, X.; Ouyang, M. Investigating relationshipInternalshortCircuit thermal runawayLithiumionBatteries thermal abuse condition. *Energy Storage Materials* **2021**, *34*, 563–573. https://doi.org/https://doi.org/10.1016/j.ensm.2020.10.020.

(22) Feng, X.; Ren, D.; He, X.; Ouyang, M. MitigatingThermalRunaway Lithium-Ion Batteries. *Joule* **2020**, *4* (4), 743–770. https://doi.org/https://doi.org/10.1016/j.joule.2020.02.010.

(23) Feng, X.; Zheng, S.; Ren, D.; He, X.; Wang, L.; Liu, X.; Li, M.; Ouyang, M. KeyCharacteristics Thermal RunawayLiionBatteries. *Energy Procedia* **2019**, *158*, 4684–4689. https://doi.org/https://doi.org/10.1016/j.egypro.2019.01.736.

(24) Wang, D.; Zheng, L.; Li, X.; Du, G.; Feng, Y.; Jia, L.; Dai, Z. Effect high NiBatterythermalSafety. *International Journal of Energy Research* **2020**, *44* (14), 12158–12168. https://doi.org/https://doi.org/10.1002/er.5812.

(25) Huang, W.; Feng, X.; Han, X.; Zhang, W.; Jiang, F. Questions Answers RelatingLithiumIonBatterySafetyIssues. *Cell Reports Physical Science* **2021**, *2* (1), 100285. https://doi.org/https://doi.org/10.1016/j.xcrp.2020.100285.

(26) Nie, K.; Hong, Y.; Qiu, J.; Li, Q.; Yu, X.; Li, H.; Chen, L. InterfacesBetweenCathode ElectrolyteSolidStateLithiumBatteriesChallenges Perspectives. *Frontiers in Chemistry* **2018**, *6*, 616. https://doi.org/10.3389/fchem.2018.00616.

(27) Inoue, T.; Mukai, K. AreAllSolidStateLithiumIonBatteriesReallySafe?–Verification Differential Scanning CalorimetryAllInclusiveMicrocell. *ACS Applied Materials & Interfaces* **2017**, *9* (2), 1507–1515. https://doi.org/10.1021/acsami.6b13224.

(28) Bates, A. M.; Preger, Y.; Torres-Castro, L.; Harrison, K. L.; Harris, S. J.; Hewson, J. AresolidStatebatteriesSafer lithium-ion batteries? *Joule* **2022**, *6* (4), 742–755. https://doi.org/https://doi.org/10.1016/j.joule.2022.02.007.

(29) Gong, J.; Wang, Q.; Sun, J. Thermalanalysis nickel cobalt lithium manganeseVaryingnickelContentused lithium ion batteries. *Thermochimica Acta* **2017**, *655*, 176–180. https://doi.org/10.1016/j.tca.2017.06.022.

(30) Hou, J.; Lu, L.; Wang, L.; Ohma, A.; Ren, D.; Feng, X.; Li, Y.; Li, Y.; Ootani, I.; Han, X.; Ren, W.; He, X.; Nitta, Y.; Ouyang, M. Thermalrunaway Lithium-ion batteries employing LiN(SO 2 F) 2 -based concentrated electrolytes. *Nature Communications* **2020**, *11*, 5100. https://doi.org/10.1038/s41467-020-18868-w.

(31) Wang, Z.; Liu, J.; Wang, M.; Shen, X.; Qian, T.; Yan, C. TowardsaferSolidstateLithiummetalBatteries review. *Nanoscale Adv.* **2020**, *2* (5), 1828–1836. https://doi.org/10.1039/D0NA00174K.

(32) Chen, R.; Nolan, A. M.; Lu, J.; Wang, J.; Yu, X.; Mo, Y.; Chen, L.; Huang, X.; Li, H. TheThermalStability Lithium Solid ElectrolytesMetallicLithium. *Joule* **2020**, *4* (4), 812–821. https://doi.org/https://doi.org/10.1016/j.joule.2020.03.012.

(33) Sun, C.; Liu, J.; Gong, Y.; Wilkinson, D. P.; Zhang, J. Recentadvances all-solid-state rechargeable lithium batteries. *Nano Energy* **2017**, *33*, 363–386. https://doi.org/https://doi.org/10.1016/j.nanoen.2017.01.028.

(34) Zhao, Y.; Yan, J.; Cai, W.; Lai, Y.; Song, J.; Yu, J.; Ding, B. Elastic well-aligned ceramic LLZO nanofiber based electrolytesSolidstateLithiumbatteries. *Energy Storage*

Materials **2019**, *23*, 306–313. https://doi.org/https://doi.org/10.1016/j.ensm.2019.04.043.

(35) Lu, W.; Xue, M.; Zhang, C. ModifiedLi7La3Zr2O12(LLZO) LLZO-polymer compositesSolidstateLithiumbatteries. *Energy Storage Materials* **2021**, *39*, 108–129. https://doi.org/https://doi.org/10.1016/j.ensm.2021.04.016.

(36) Fu, K.; Gong, Y.; Dai, J.; Gong, A.; Han, X.; Yao, Y.; Wang, C.; Wang, Y.; Chen, Y.; Yan, C.; Li, Y.; Wachsman, E.; Hu, L. Flexible,solidState,ionConductingmembrane 3D garnet nanofiber networksLithiumbatteries. *Proceedings of the National Academy of Sciences* **2016**, *113*, 201600422. https://doi.org/10.1073/pnas.1600422113.

(37) Yang, C.-P.; Liu, B.; Jiang, F.; Zhang, Y.; Xie, H.; Hitz, E.; Hu, L. Garnet/polymerhybridIonconductingProtectivelayer stable lithium metal anode. *Nano Research* **2017**, *10*, 1–10. https://doi.org/10.1007/s12274-017-1498-2.

(38) Yoshima, K.; Harada, Y.; Takami, N. ThinhybridElectrolytebased garnet-type lithium-ion conductor Li7La3Zr2O1212 VclassBipolarbatteries. *Journal of Power Sources* **2016**, *302*, 283–290. https://doi.org/https://doi.org/10.1016/j.jpowsour.2015.10.031.

(39) Takami, N.; Yoshima, K.; Harada, Y. 12VClassBipolarLithiumIonBatteriesUsingLi4Ti5O12Anode Low-Voltage System Applications. *Journal of The Electrochemical Society* **2016**, *164* (1), A6254–A6259. https://doi.org/10.1149/2.0421701jes.

(40) RTCA *Minimum Operational Performances Standards Rechargeable Lithium Battery and Battery Systems (DO311)*; RTCA DO-311; Washington, DC 2017.

(41) Finegan, D. P.; Tjaden, B.; Heenan, T. M. M.; Jervis, R.; Michiel, M. D.; Rack, A.; Hinds, G.; Brett, D. J. L.; Shearing, P. R. TrackingInternalTemperature Structural DynamicsNailPenetration Lithium-Ion Cells. *Journal of The Electrochemical Society* **2017**, *164* (13), A3285–A3291. https://doi.org/10.1149/2.1501713jes.

(42) Gholizadeh, S. Areview non-destructive testing methodsCompositematerials. *Procedia Structural Integrity* **2016**, *1*, 50–57. https://doi.org/https://doi.org/10.1016/j.prostr.2016.02.008.

(43) Finegan, D.; Scheel, M.; Robinson, J.; Tjaden, B.; Hunt, I.; Mason, T.; Millichamp, J.; Di Michiel, M.; Offer, G.; Hinds, G.; Brett, D. J. L.; Shearing, P. InoperandoHighspeedTomography lithium-ion batteriesThermalrunaway. *Nature Communications* **2015**, *6*, 6924. https://doi.org/10.1038/ncomms7924.

(44) Finegan, D. P.; Darst, J.; Walker, W.; Li, Q.; Yang, C.; Jervis, R.; Heenan, T. M. M.; Hack, J.; Thomas, J. C.; Rack, A.; Brett, D. J. L.; Shearing, P. R.; Keyser, M.; Darcy, E. Modelling experimentsIdentifyhighRiskfailureScenarios testingSafety lithium-ion cells. *Journal of Power Sources* **2019**, *417*, 29–41. https://doi.org/https://doi.org/10.1016/j.jpowsour.2019.01.077.

(45) Finegan, D.; Darcy, E.; Keyser, M.; Tjaden, B.; Heenan, T.; Jervis, R.; Bailey, J.; Vo, N. T.; Magdysyuk, O.; Drakopoulos, M.; Di Michiel, M.; Rack, A.; Hinds, G.; Brett, D. J. L.; Shearing, P. Identifying CauseRupture Li-Ion BatteriesThermalRunaway. *Advanced Science* **2018**, *5*, 1700369. https://doi.org/10.1002/advs.201700369.

(46) Finegan, D. P.; Darcy, E.; Keyser, M.; Tjaden, B.; Heenan, T. M. M.; Jervis, R.; Bailey, J. J.; Malik, R.; Vo, N. T.; Magdysyuk, O. V.; Atwood, R.; Drakopoulos, M.; DiMichiel, M.; Rack, A.; Hinds, G.; Brett, D. J. L.; Shearing, P. R. CharacterisingthermalRunaway lithium-ion cellsInducing monitoring internal short circuits. *Energy Environ. Sci.* **2017**, *10* (6), 1377–1388. https://doi.org/10.1039/C7EE00385D.

(47) Walker, W. Q.; Darst, J. J.; Finegan, D. P.; Bayles, G. A.; Johnson, K. L.; Darcy, E. C.; Rickman, S. L. Decoupling heat generatedEjected non-ejected contents18650formatLithiumionCellsusingStatisticalmethods. *Journal of Power Sources* **2019**, *415*, 207–218. https://doi.org/https://doi.org/10.1016/j.jpowsour.2018.10.099.

(48) Smith, A. J.; Burns, J. C.; Zhao, X.; Xiong, D.; Dahn, J. R. AHighPrecisionCoulometryStudy SEI GrowthLi/GraphiteCells. *Journal of The Electrochemical Society* **2011**, *158* (5), A447. https://doi.org/10.1149/1.3557892.

(49) Jones, J.; Anouti, M.; Caillon-Caravanier, M.; Willmann, P.; Sizaret, P.-Y.; Lemordant, D. Solubilization SEI lithium saltsAlkylcarbonatesolvents. *Fluid Phase Equilibria* **2011**, *305* (2), 121–126. https://doi.org/https://doi.org/10.1016/j.fluid.2011.03.007.

(50) Somerville, L.; Bareño, J.; Jennings, P.; McGordon, A.; Lyness, C.; Bloom, I. TheEffect Pre-Analysis WashingSurfaceFilm Graphite Electrodes. *Electrochimica Acta* **2016**, *206*, 70–76. https://doi.org/https://doi.org/10.1016/j.electacta.2016.04.133.

(51) Scharner, S. QuantitativesafetyCharacterization li-ion cells. In *JRC Exploratory Research Workshop*; 2018.

Figure list:

Table list: